Research Article

ADVANCED PHOTONICS NEXUS

Random fiber laser using a cascaded fiber loop mirror

Ming Shen,[a,b] **Yanxin Li**,[a,b] **Qianying Li**,[a,b] **and Xuewen Shu**[a,b,*]
[a]Huazhong University of Science and Technology, Wuhan National Laboratory for Optoelectronics, Wuhan, China
[b]Huazhong University of Science and Technology, School of Optical and Electronic Information, Wuhan, China

Abstract. Random fiber lasers (RFLs) have attracted extensive attention due to their rich physical properties and wide applications. Here, a RFL using a cascaded fiber loop mirror (CFLM) is proposed and presented. A CFLM with 10 fiber loop mirrors (FLMs) is simulated by the transfer matrix method and used to provide random feedback. Multiple spikes are observed in both the simulated and measured reflection spectra. The RFL operates in a single longitudinal mode near the threshold and a time-varying multilongitudinal mode at higher pump powers. The RFL exhibits a time-varying radio-frequency spectrum. The Lévy–Gaussian distribution transition is observed, as in many RFLs. The operation mechanism of the lasing longitudinal modes and the impact of complex mode competition and mode hopping on the output characteristics are discussed through experimental and theoretical results. In this study, we unveil an artificial random feedback structure and pave another way for the realization of RFLs, which should be a platform for multidisciplinary studies in complex systems.

Keywords: random fiber lasers; fiber loop mirrors; artificial scattering media.

Received Feb. 14, 2024; revised manuscript received Mar. 31, 2024; accepted for publication Apr. 22, 2024; published online May 16, 2024.

[DOI: 10.1117/1.APN.3.3.036009]

1 Introduction

Random lasers have attracted extensive attention due to their rich physical properties[1,2] and multiple applications such as sensing,[3,4] imaging,[5–7] optical communication,[8,9] and nonlinear frequency generation.[10] This kind of laser employs a highly scattering medium to confine the light, unlike the well-defined mirrors in conventional lasers. Therefore, random lasers possess a relatively simple cavity structure and are cost-effective. Among them, random fiber lasers (RFLs) blend together the attractive features of random lasers and fiber lasers and become a new breed of light source with simplicity of fabrication, good directionality, high efficiency, and high stability.[11] The first RFL was achieved by inserting the suspension of rutile particles in a rhodamine 6G solution into a hollow core photonic crystal fiber.[12] Since then, researchers have developed many ways to achieve RFLs. One of the most commonly used techniques is the Rayleigh scattering induced by the refractive index fluctuations of long (several kilometers) fiber. Such RFLs conveniently use the Raman effect and break the spectral limitation of active fibers but still suffer from the watt-level threshold.[13,14] Using the rare-earth-doped fiber and a half-open cavity with one mirror can significantly reduce the lasing threshold, but the required long fiber is still a main drawback of such lasers.[15,16] One way to shorten the fiber length is changing the common single-mode fiber to fibers with stronger Rayleigh scattering, such as polarization-maintaining fiber[17] and photonic crystal fiber.[18]

In recent years, a variety of artificial scattering media with enhanced scattering has been proposed and demonstrated to be good candidates for random lasing. They further shorten the required fiber length to a meter level. Different kinds of polymer fibers have been proposed to achieve random lasing. Researchers doped dye molecules,[19] ferromagnetic nanoparticles,[20] and scattering nanoparticles[21] into polymer fibers to tune the random lasing behavior. Other works such as self-healing hydrogel fiber based on a metal–organic framework[22] and nanowire composite doped with TiN nanoparticles[23] also provide great tunability to the RFL. But these works could require a relatively complex fabrication process. The development of laser micromachining greatly enhances the fabrication flexibility of

*Address all correspondence to Xuewen Shu, xshu@hust.edu.cn

artificial scattering media. A random phase-shift fiber Bragg grating (FBG) is fabricated with the beam-scanning method and used to achieve narrow bandwidth RFL.[24] The femtosecond direct-writing technique can induce refractive index inhomogeneities in the fiber core to enhance the Rayleigh scattering.[25] Extensive studies based on random fiber gratings have been conducted, such as single-frequency random lasing,[26] lasing mode selection,[27] and high-power single-peak Raman RFLs.[28] A random Fabry–Pérot (F-P) cavity array based on Au-film-coated fiber reflector is another choice for random lasing by light localization.[29] Although these artificial scattering media provide much fabrication flexibility, the requirement of specific expensive fabrication equipment hinders further application. Therefore, finding new cost-effective artificial scattering media with ease of fabrication would greatly facilitate the application of RFLs. Moreover, it is of significant interest to enrich the RFL category because it has become an important platform for multidisciplinary studies where Lévy statistics,[30] replica symmetry breaking,[31] optical turbulence-like behavior,[32] and temporal optical rogue waves[33] are found and discussed.

In this paper, we propose and demonstrate a novel RFL based on a cascaded fiber loop mirror (CFLM). Fiber loop mirrors (FLMs) are commonly used as broadband fiber mirrors.[34] Here, we cascaded up to 10 FLMs (10-CFLM) to obtain a chaotic reflection spectrum with greatly enhanced reflectivity. The transmission and reflection characteristics of the CFLM were simulated by the transfer matrix method and coincided well with the measured results. Random lasing with a 10-CFLM was achieved and the Lévy–Gaussian distribution transition was observed. The RFL operated in the single longitudinal mode (SLM) near the threshold and time-varying multilongitudinal mode at high pump powers. Complex lasing behaviors at different pump powers with different numbers of FLMs were discussed. Theoretical analysis shows the operation mechanism of intracavity lasing longitudinal modes, where complex mode competition and mode hopping have a great influence on the output characteristics.

2 Experimental Setup

2.1 CFLM Simulation and Characterization

The schematic of the CFLM is shown in Fig. 1(a). The FLM is made by connecting the two ports on the same side of a fiber coupler. Several FLMs with fiber loop length L_c are connected in series with adjacent distance L_f. The transmission and reflection characteristics of the cascaded FLM can be analyzed by the transfer matrix method. As shown in the dotted box in Fig. 1(a), an FLM with two ports can be described as[35]

$$\begin{bmatrix} E_1^+ \\ E_1^- \end{bmatrix} = \frac{1}{(1-2k)(1-\gamma)} \times \begin{bmatrix} e^{(\alpha_f - j\beta)L_c} & -2j(1-\gamma)\sqrt{k(1-k)} \\ 2j(1-\gamma)\sqrt{k(1-k)} & (1-\gamma)^2 e^{(-\alpha_f + j\beta)L_c} \end{bmatrix} \begin{bmatrix} E_2^+ \\ E_2^- \end{bmatrix}, \tag{1}$$

where k is the coupler coupling constant, γ is the excess loss induced by the coupler, α_f is the field loss, and β is the propagation constant. E is the electric field amplitude, and the superscripts "+ and −" represent the right and left going waves, respectively. The single-mode fiber connecting the adjacent FLMs can be described as[35]

$$\begin{bmatrix} E_1^+ \\ E_1^- \end{bmatrix} = \begin{bmatrix} e^{(\alpha_f - j\beta)L_f} & 0 \\ 0 & e^{(-\alpha_f + j\beta)L_f} \end{bmatrix} \begin{bmatrix} E_2^+ \\ E_2^- \end{bmatrix}. \tag{2}$$

The reflection spectrum becomes more chaotic as the number of FLMs increases. For simplicity, we choose 10 FLMs, and the k, γ, and L_c of them are set to 0.01, 0.015, and 0.4 m, respectively. Each FLM has a calculated reflectivity of ~3.8%, which yields a moderate reflectivity and transmissivity after the cascade operation. Nine adjacent distance L_f are randomly distributed from 0.3 to 1 m, which are 0.35, 0.31, 0.65, 0.45, 0.86, 0.69, 0.52, 0.66, and 0.59 m, and they add up to 5.08 m. The fiber fusion loss of 0.999 is used to replace the small loss of fiber. The calculated reflection spectrum is shown in Fig. 1(b) with a wavelength step of 0.01 pm, where the maximum reflectivity is 79.1% at the wavelength λ_1 (1549.973 nm). The chaotic spectrum has the same trend as other reported random media.[29,36] The multiple spikes may support several modes in the laser, and some of the modes may prevail in the mode competition and start lasing. Figure 1(c) shows the simulated spatial intensity distribution inside the 10-CFLM by the transfer matrix method.[37] Many "hot spots" at random wavelengths are observed between the second and the sixth FLMs, which has also

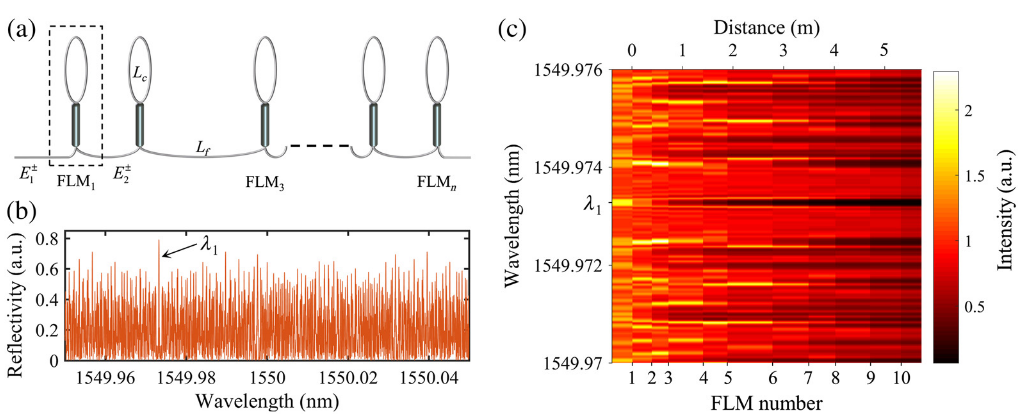

Fig. 1 (a) Schematic of the CFLM. Simulated (b) reflection spectrum and (c) spatial intensity distributions of the 10-CFLM.

been reported in other works.[38,39] The spatial intensity distribution at λ_1 follows an exponential decay, as shown in Fig. S1(a) in the Supplementary Material, which demonstrates the Anderson localization effect in the CFLM.[39]

The obvious change of the transmission and reflection characteristics of the CFLM with a small change of L_f is understandable because the effective length of the F-P cavity formed by the adjacent FLMs is changed. We further simulated the situations with fluctuating parameters L_c and k. Random errors of $[-5\ 5]$ mm and $[-0.005\ 0.005]$ were added to 10 L_c and k values, respectively. The results are shown in Figs. 2(a1) and 2(a2), respectively; Fig. 2(a3) is the enlarged view near λ_1 of Fig. 1(b) for comparison. The change of L_c changes the effective length of the F-P cavity, thereby changing the reflection spectrum of the CFLM. The reflection spectrum is highly sensitive to the cavity length and has a totally different characteristic, as shown in Fig. 2(a1). However, the k only influences the reflectivity of the FLM and causes the overall rise or fall of the spectrum, as shown in Fig. 2(a2). To fabricate such a CFLM, we first choose 10 single-mode fiber couplers with the same coupling constant ($k = 0.01$) and make each of them form an FLM with a loop length L_c of 0.4 m by splicing two ports of each coupler. Then, we splice these 10 FLMs one by one according to the adjacent distances designed above. We measured the transmission and reflection spectra of the 10-CFLM with a light-wave measurement system (8164A, Agilent, Santa Clara, CA, U. S.). Figure 2(b) shows the measured results with 0.1 pm resolution. The larger wavelength step results in missing some details, but multiple spikes can still be observed. The enlarged view of the 40 pm span in Fig. 2(b3) shows random spikes with spacings of the pm level. The mean transmissivity T is $\sim$0.48, and the localization length, ξ calculated from the equation $\xi = L/2\ \ln(1/T)$,[40] is $0.69L$, where L is the effective length of the 10-CFLM. The Anderson localization effect should appear in the proposed 10-CFLM, since the localization length is smaller than the effective length.[39]

2.2 Laser Setup

The setup of the proposed RFL is illustrated in Fig. 3. The pump source is a 976 nm laser diode (LD) and is coupled into the cavity through a wavelength division multiplexer (WDM). An FBG with 1550 nm center wavelength, 63% peak reflectivity, and 50 pm full width at half-maximum (FWHM) is used to select the lasing wavelength. The CFLM provides random feedback and is inserted between a commercial erbium-doped fiber (EDF, I-25, Fibercore, Southampton, U. K., 1.5 m) and an isolator. The laser outputs after the isolator.

3 Laser Characterization

The 10-CFLM was used first in the experiment. Figure 4(a) shows the output spectra measured using an optical spectrum analyzer (OSA, AQ6370C, Yokogawa, Tokyo, Japan) with a 4-pm sampling interval. The optical signal-to-noise ratio reaches as high as 65 dB at the maximum pump power of 168 mW, and the FWHM remains below 20 pm. The output spectrum may show an abrupt deviation from the stable bell-shaped profile to a flat-top profile when we increase the pump power, as shown in the inset of Fig. 4(a). However the output spectrum will eventually stabilize to the same as in Fig. 4(a). Figure 4(b) shows the output power curve of the RFL, and the threshold is below 15 mW. The measured results follow a linear distribution, and the slope efficiency is $\sim$2.5%.

We measured the longitudinal mode performance using a confocal scanning F-P interferometer (SFPI, SA200-12B, Thorlabs, Newton, NJ, U. S., 1.5 GHz FSR). Figure 5(a1) shows that the RFL operates in the SLM at low pump powers (22 mW), which has also been reported in other RFLs.[38,41,42] The SLM operation maintains a pump power range from the threshold to $\sim$40 mW. When we further increase the pump power (75 mW), the measured result changes to a time-varying random multilongitudinal mode operation, as typically shown in Figs. 5(a2) and 5(a3). This result is highly sensitive to environmental changes such as wind. The longitudinal mode envelopes would only change their amplitude at the moment we increase the pump power, and then, new modes would appear. The working principle could be as follows. Higher gain is provided by higher pump powers, which is first experienced by the existing longitudinal modes. Then, more longitudinal modes start to oscillate under higher gain and compete for the pump in the EDF,[43] which also explains the reason for the flat-top spectrum in the inset of Fig. 4(a). The radio-frequency spectrum is measured using an electrical spectrum analyzer (FSH20, Rohde & Schwarz, Munich, Germany) and averaged by 20 measurements, as shown in Fig. 5(b). The averaged beat peaks are different from

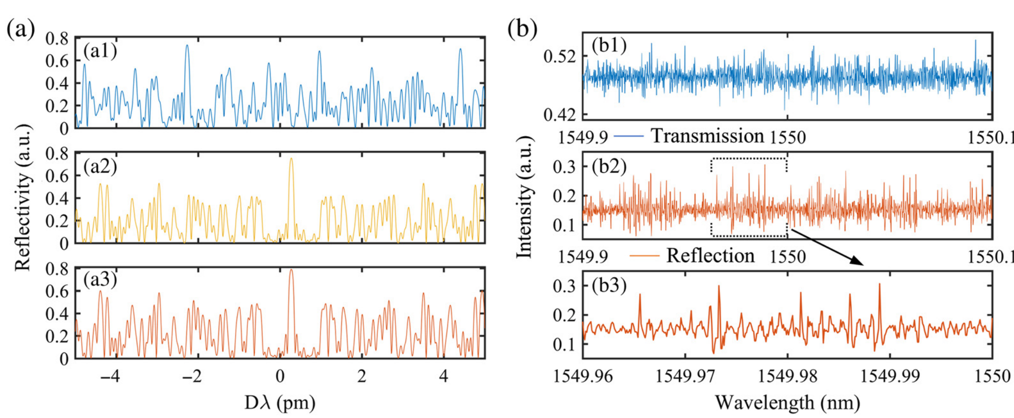

Fig. 2 Simulated reflection spectra of the 10-CFLM at λ_1 with (a1) fluctuating L_c, (a2) fluctuating k, and (a3) enlarged view of Fig. 1(b) for comparison. Experimentally measured (b1) transmission and (b2) reflection spectra of the 10-CFLM. (b3) Enlargement of panel (b2).

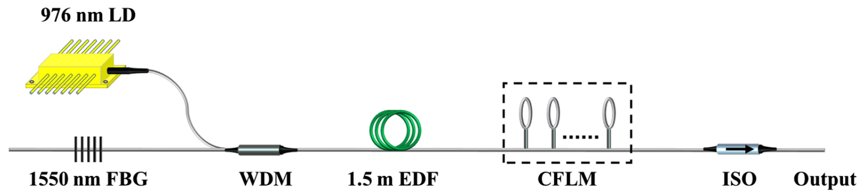

Fig. 3 Experimental setup. LD, laser diode; WDM, wavelength division multiplexer; EDF, erbium-doped fiber; CFLM, cascaded fiber loop mirror; ISO, isolator.

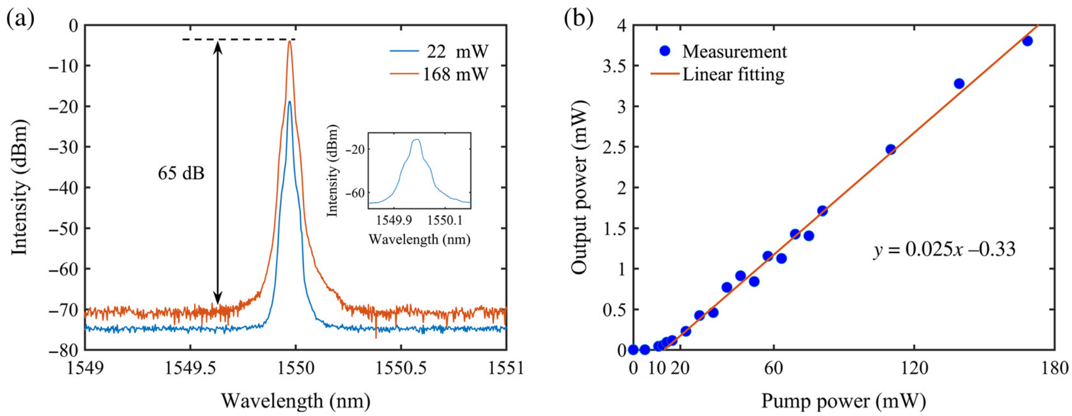

Fig. 4 (a) Output spectra at the pump powers of 22 and 168 mW. Inset is the output spectrum right after the increase of pump power. (b) Output power versus pump power.

every single measurement because of the time-varying random multilongitudinal mode operation and the slow response speed of the electrical spectrum analyzer. Each single measurement exhibits some different beat peaks, as shown in Fig. S2(c) in the Supplementary Material, and caused the small peak intensity after the average operation. To further understand the measured results, we collected the time series and applied the Fourier transform to obtain the frequency information, which shows similar time-varying beat peaks (details in Sec. A in the Supplementary Material).

Recently, a transition from Gaussian to Lévy to Gaussian distribution of the spectral intensity dynamics has been observed in many RFLs, where the change happens around the lasing threshold.[30,44,45] The distribution of spectral intensity dynamics can be described by the Lévy index $\alpha \in (0,2]$. The Gaussian distribution is with $\alpha = 2$, and the Lévy distribution is with $0 < \alpha < 2$. Here, we measured 1200 output spectra in an hour at different pump powers and calculated the probability density function (PDF) of the peak spectral intensity. The α-stable Lévy distribution is fitted to the PDF, and the variation of the index α is plotted in Fig. 6. The Lévy distribution ($\alpha < 2$) appears around the lasing threshold (15 mW), and the Gaussian distribution ($\alpha = 2$) appears below and well above the threshold.

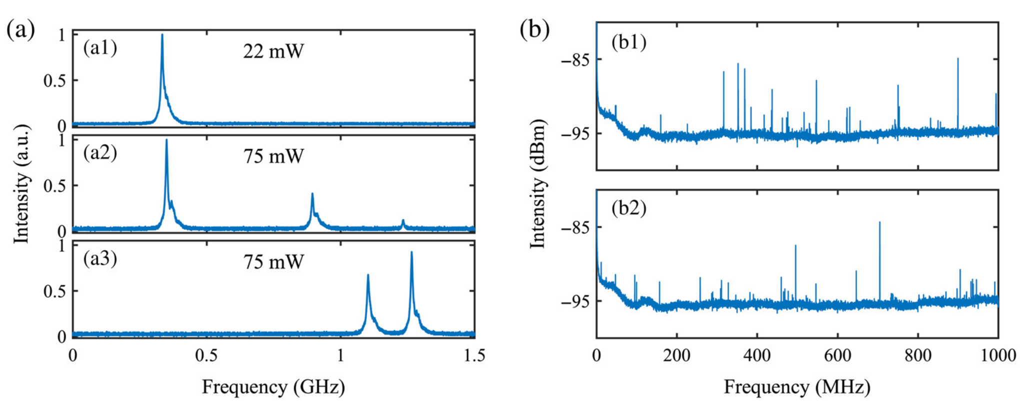

Fig. 5 Longitudinal mode envelopes under the pump powers of (a1) 22 mW and (a2) and (a3) 75 mW. (b) Averaged radio-frequency spectra at two different times at the pump power of 168 mW.

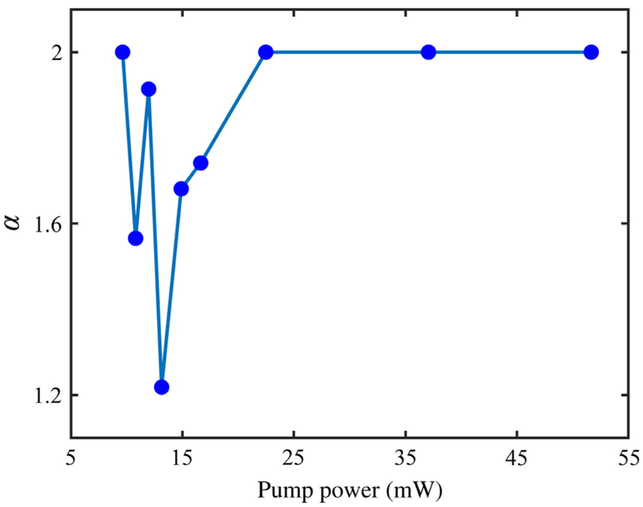

Fig. 6 Variation of the Lévy index α with pump power.

It is obvious that more FLMs provide more randomness. When there is only one FLM, the laser cavity length is fixed, and a conventional laser is formed. Its radio-frequency spectrum is shown in Fig. 7(a1), and the peak at 18.41 MHz corresponds to a calculated cavity length of ~11.24 m. When the number of FLMs increases, any two FLMs form a subcavity, and the Vernier effect between them filters the lasing modes.[35] When there is only a small number of FLMs, three for instance (3-CFLM), the reflection spectrum is still of high regularity (Fig. S3 in the Supplementary Material). We chose the first three FLMs of the 10-CFLM ($L_f = 0.35$, 0.31 m); the averaged radio-frequency spectrum is shown in Fig. 7(a2). The circle-marked peak at 128.7 MHz corresponds to a calculated cavity length of ~1.61 m, which equals the length of the F-P cavity formed by the first two FLMs. The first two FLMs play the leading role because the former FLMs reflect more of the laser. The peak at 18.41 MHz (with one FLM) is not seen because of the mismatch among different cavity lengths. Many lower peaks appear around the maximum peak, which is further discussed in Sec. B in the Supplementary Material. The measured longitudinal mode envelopes in Fig. 7(b) show more modes than Fig. 5(a) because more longitudinal modes could oscillate with the 3-CFLM (Sec. B in the Supplementary Material), while for 10-CFLM, the reflection spectrum shows a chaotic feature, and the spacing of some reflection peaks may be comparable to the FWHM of the FBG used. Then, most longitudinal modes would be filtered out by the joint action of the CFLM and FBG. The small number of lasing modes and the time-varying mode operation make it hard for the real-time measurement of the beat peaks. Nevertheless, the reflection spectrum is highly sensitive to changes in fiber length, according to the simulation. The longitudinal mode with the highest gain in the FWHM of the FBG used would change with time and result in the time-varying random multilongitudinal mode behavior.

4 Longitudinal Mode Simulation

We further simulated the lasing condition in the proposed RFL within a bandwidth of 2.5 GHz (20 pm) centered at the maximum reflectivity (λ_1) in Fig. 1(b). The lasing longitudinal mode should satisfy both the phase and gain–loss conditions.[41,46] Modes of different frequencies are scattered back from the CFLM with different phase values, and their phase profile, φ_{CFLM}, can be calculated from the reflection spectrum. Then, the phase condition can be described as

$$\varphi_{\mathrm{FBG}} + \frac{nl}{\lambda} 2\pi + \varphi_{\mathrm{CFLM}} = 2\pi m, \tag{3}$$

where the phase of FBG φ_{FBG} is π,[41] the refractive index n is 1.45, the cavity length l is 10.84 m, and m is an integer. The gain–loss condition is

$$R_{\mathrm{FBG}} + G + R_{\mathrm{CFLM}} \geq 0, \tag{4}$$

where R_{FBG} is the measured reflectivity of the FBG, G is the gain in one round trip, and R_{CFLM} is the simulated reflectivity of the CFLM. The results for phase condition are shown in Figs. 8(a) and 8(b), where the red points correspond to the lasing modes. Up to 78 modes in the bandwidth of 2.5 GHz satisfy the phase condition, and each of them could compete in the lasing condition. The adjacent mode spacing is about tens of megahertz, and therefore, the spacing between any two modes could be hundreds of megahertz, which coincides well with the beat peaks in Fig. 5(b). We applied the gain–loss condition to these 78 modes and counted the number of lasing modes versus G, as shown in Fig. 8(c). The first mode begins to oscillate at the G of 4.3 dB, and the second mode appears at the G of 4.7 dB,

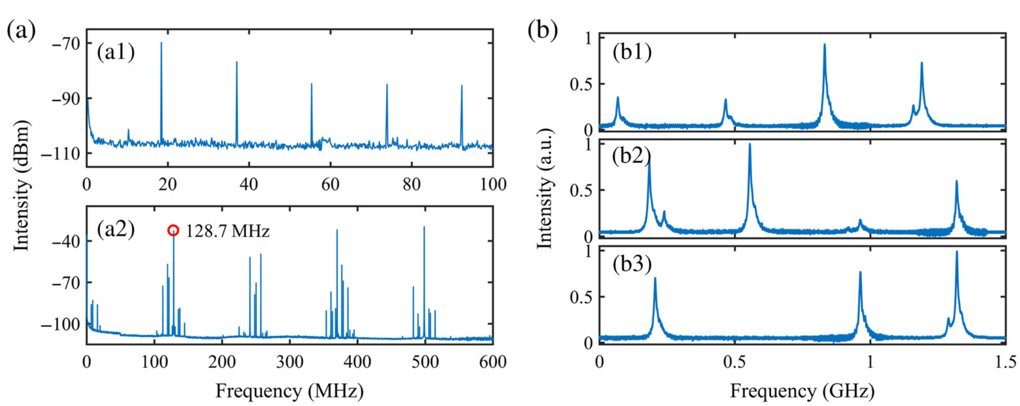

Fig. 7 Radio-frequency spectra with (a1) one and (a2) three FLMs. (b) Longitudinal mode envelopes with three FLMs at different times.

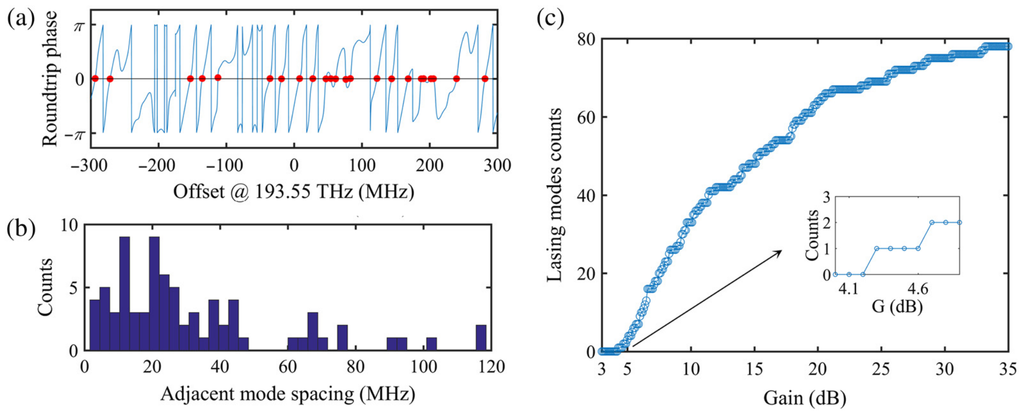

Fig. 8 (a) Simulated phase of the electromagnetic field after a round trip as a function of frequency (offset from 193.55 THz). The red points are the solutions of phase conditions. (b) Adjacent longitudinal mode spacing counts from phase conditions. (c) Lasing modes count at different gains. Inset is the enlargement near the G of 4 dB. The simulation bandwidth is 2.5 GHz (20 pm).

which corresponds to the SLM operation at low pump powers near the threshold. The number of lasing modes keeps increasing and reaches the ultimate number of 78 at the G of 33.2 dB, where all modes are excited by the sufficiently high pump power. Because no specific techniques were applied to mitigate the homogeneous broadening effect of the EDF, the mode competition and mode hopping[16,38,43] could appear. Together with the high sensitivity of the CFLM to the environment, they resulted in a time-varying gain curve (G). Then, the number of lasing modes would also be time-varying, which led to the time-varying results in Fig. 5.

5 Conclusion

In conclusion, we proposed and demonstrated a novel RFL based on the CFLM. The transmission and reflection characteristics of the CFLM were analyzed by the transfer matrix method. The experimentally measured results showed a chaotic spectrum with many narrow spikes, which coincides well with the simulation results. The 10-CFLM met the requirement of Anderson localization. Such an RFL also obeyed the Lévy–Gaussian distribution transition observed in many RFLs. The proposed RFL operated in a stable SLM at low pump powers. Further increasing the pump power, the RFL operated in a time-varying multilongitudinal mode. Different numbers of FLMs were applied and discussed. Theoretical analysis of lasing modes provides evidence for the SLM operation and reveals the impact of complex mode competition and mode hopping on the output characteristics.

Nowadays, a variety of random feedback structures have been proposed to promote the development and application of RFLs. The CFLM in this work is a completely new and random feedback structure other than the scattering-enhanced special fibers and laser micromachined devices. It is composed of commonly used fiber couplers and connected by a fiber fusion operation and thus does not require any complex fabrication process or expensive fabrication equipment. In addition, the proposed CFLM can be theoretically simulated in detail to better reveal its effect on the RFL. The radio-frequency spectra show interesting phenomena due to the multiple F-P cavities formed in the CFLM, which is briefly discussed here and worth further investigating in the future. Compared with the recent work where 11 fiber reflectors with Au-film-coated facets are connected in series through flanges,[29] the CFLM based on fiber fusion operation should have better reusability for superresolution spectroscopy applications. The weak saturable absorption effect in each FLM, also known as a nonlinear optical loop mirror,[47] provides a platform for the analysis of cascaded effects for pulsating operation. Further changes to the fiber loop section can provide more functions, such as a stronger saturable absorption effect with active gain[48] and optical switching with injected control light.[49] The proposed RFL may be a good candidate for the random bit generation[50] after increasing the number of intracavity modes with broadband FBGs or reflectors. Multiple modifications in the cascade operation should provide interesting results and are worth the effort. The proposed CFLM enriches the RFL category and should be a novel platform for multidisciplinary studies in complex systems, which has good potential for scientific research and practical applications.

Disclosures

The authors declare no conflict of interest.

Code and Data Availability

Data underlying the results presented in this paper are not publicly available at this time but may be obtained from the authors upon reasonable request.

Acknowledgments

This work was supported by the National Key R&D Program of China (Grant No. 2023YFE0105800), the National Natural Science Foundation of China (Grant Nos. 62275093 and 61775074), and the Key R&D Program of Hubei Province (Grant No. 2021BAA036).

References

1. D. V. Churkin et al., "Recent advances in fundamentals and applications of random fiber lasers," *Adv. Opt. Photonics* **7**(3), 516–569 (2015).
2. A. S. L. Gomes et al., "Recent advances and applications of random lasers and random fiber lasers," *Prog. Quantum Electron.* **78**, 100343 (2021).

3. J. Deng et al., "Random fiber laser based on a partial-reflection random fiber grating for high temperature sensing," *Opt. Lett.* **46**(5), 957–960 (2021).
4. B. Han et al., "Ultralong single-ended random fiber laser and sensor," *Laser Photonics Rev.* **17**(6), 2200797 (2023).
5. R. Gayathri et al., "Plasmonic random laser enabled artefact-free wide-field fluorescence bioimaging: uncovering finer cellular features," *Nanoscale Adv.* **4**(10), 2278–2287 (2022).
6. S. Wang et al., "High-power multimode random fiber laser for speckle-free imaging," *Ann. Phys.* **533**(12), 2100390 (2021).
7. H. Wu et al., "Temporal ghost imaging with random fiber lasers," *Opt. Express* **28**(7), 9957–9964 (2020).
8. X. Y. Ma et al., "Vortex random fiber laser with controllable orbital angular momentum mode," *Photonics Res.* **9**(2), 266–271 (2021).
9. X. Shi et al., "Selectively visualizing the hidden modes in random lasers for secure communication," *Laser Photonics Rev.* **15**(10), 2100295 (2021).
10. B. Hu et al., "Highly efficient octave-spanning long-wavelength infrared generation with a 74% quantum efficiency in a χ^2 waveguide," *Nat. Commun.* **14**, 7125 (2023).
11. S. K. Turitsyn et al., "Random distributed feedback fibre laser," *Nat. Photonics* **4**(4), 231–235 (2010).
12. C. J. de Matos et al., "Random fiber laser," *Phys. Rev. Lett.* **99**(15), 153903 (2007).
13. R. Ma et al., "Robust 1.69 μm random fiber laser with high spectral purity based on ordinary fibers," *J. Lightwave Technol.* **40**(12), 3942–3946 (2022).
14. S. Li et al., "Multi-wavelength random fiber laser with a spectral-flexible characteristic," *Photonics Res.* **11**(2), 159–164 (2023).
15. M. Shen et al., "Multi-wavelength random fiber laser based on a tilted parallel inscribed apodized fiber Bragg grating array," *Opt. Lett.* **47**(21), 5473–5476 (2022).
16. J. Lv et al., "Tailoring the spectrum and spatial mode of Yb-doped random fiber laser," *Opt. Express* **30**(5), 8345–8355 (2022).
17. H. Wang et al., "Acoustic wave coupling in dual-wavelength orthogonal polarized Brillouin random fiber laser using polarization-maintaining fiber," *J. Lightwave Technol.* **40**(8), 2541–2547 (2022).
18. J. He et al., "Supercontinuum generation directly from a random fiber laser based on photonic crystal fiber," *Opt. Express* **28**(19), 27308–27315 (2020).
19. V. D. Ta et al., "Flexible and tensile microporous polymer fibers for wavelength-tunable random lasing," *Nanoscale* **12**(23), 12357–12363 (2020).
20. W. Du et al., "Thermal treatment effect on the random lasing polarization of polymer optical fiber," *Opt. Laser Technol.* **149**, 107855 (2022).
21. J. Xia et al., "Tunable replica symmetry breaking in random laser," *Nanophotonics* **12**(4), 761–771 (2023).
22. D. Zhu et al., "Metal-organic framework-based self-healing hydrogel fiber random lasers," *Nanoscale* **15**(25), 10685–10692 (2023).
23. J. Lyu et al., "Low-threshold and narrow-emission random lasing in a self-assembly tin nanoparticle-doped carbon quantum dot/DCM nanowire composite," *Photonics Res.* **10**(9), 2239–2246 (2022).
24. A. Zhang et al., "Investigation of narrow band random fiber ring laser based on random phase-shift Bragg grating," *Opt. Laser Technol.* **116**, 1–6 (2019).
25. A. Dostovalov et al., "Continuous and discrete-point Rayleigh reflectors inscribed by femtosecond pulses in singlemode and multimode fibers," *Opt. Laser Technol.* **167**, 109692 (2023).
26. J. C. Deng et al., "Single-frequency random distributed Bragg reflector fiber laser," *J. Lightwave Technol.* **40**(13), 4385–4390 (2022).
27. W. L. Zhang et al., "Temperature-controlled mode selection of Er-doped random fiber laser with disordered Bragg gratings," *Photonics Res.* **4**(3), 102–105 (2016).
28. J. C. Deng et al., "High-power random Raman fiber laser with an ultrashort random fiber grating," *J. Lightwave Technol.* **40**(8), 2535–2540 (2022).
29. Y. Zhang et al., "Coherent random fiber laser-enabled super-resolution spectroscopy," *ACS Photonics* **10**(8), 2670–2678 (2023).
30. H. Wang et al., "Stabilizing Brillouin random laser with photon localization by feedback of distributed random fiber grating array," *Opt. Express* **30**(12), 20712–20724 (2022).
31. L. Zhang et al., "Transient replica symmetry breaking in Brillouin random fiber lasers," *PhotoniX* **4**(1), 33 (2023).
32. I. R. R. Gonzalez et al., "Turbulence hierarchy in a random fibre laser," *Nat. Commun.* **8**(1), 15731 (2017).
33. J. Xu et al., "Optical rogue wave in random fiber laser," *Photonics Res.* **8**(1), 1–7 (2020).
34. Y. Wang et al., "Tunable pulsed dysprosium laser within a continuous range of 545 nm around 3 μm," *J. Lightwave Technol.* **40**(14), 4841–4847 (2022).
35. J. Capmany and M. A. Muriel, "A new transfer matrix formalism for the analysis of fiber ring resonators: compound coupled structures for FDMA demultiplexing," *J. Lightwave Technol.* **8**(12), 1904–1919 (1990).
36. M. I. Skvortsov et al., "Narrow-linewidth Er-doped fiber lasers with random distributed feedback provided by artificial Rayleigh scattering," *J. Lightwave Technol.* **40**(6), 1829–1835 (2022).
37. M. A. Muriel, A. Carballar, and J. Azana, "Field distributions inside fiber gratings," *IEEE J. Quantum Electron.* **35**(4), 548–558 (1999).
38. B. Lv et al., "Low frequency-noise ring random fiber laser with a dual-cavity FBG Fabry–Pérot filter," *J. Lightwave Technol.* **40**(15), 5286–5293 (2022).
39. J. Deng et al., "Stable and low-threshold random fiber laser via Anderson localization," *Opt. Express* **27**(9), 12987–12997 (2019).
40. V. Milner and A. Z. Genack, "Photon localization laser: low-threshold lasing in a random amplifying layered medium via wave localization," *Phys. Rev. Lett.* **94**(7), 073901 (2005).
41. P. Tovar, G. Temporao, and J. P. von der Weid, "Longitudinal mode dynamics in SOA-based random feedback fiber lasers," *Opt. Express* **27**(21), 31001–31012 (2019).
42. M. Gagne and R. Kashyap, "Demonstration of a 3 mW threshold Er-doped random fiber laser based on a unique fiber Bragg grating," *Opt. Express* **17**(21), 19067–19074 (2009).
43. L. Dang et al., "Tens of hertz ultra-narrow linewidth fiber ring laser based on external weak distributed feedback," *Opt. Express* **30**(19), 34575–34585 (2022).
44. J. Li et al., "Lévy spectral intensity statistics in a Raman random fiber laser," *Opt. Lett.* **44**(11), 2799–2802 (2019).
45. S. Jagannathan et al., "Random lasing from optical fibers with phase separated glass cores," *Opt. Express* **28**(15), 22049–22063 (2020).
46. A. Consoli, N. Caselli, and C. López, "Electrically driven random lasing from a modified Fabry–Pérot laser diode," *Nat. Photonics* **16**(3), 219–225 (2022).
47. K. Krupa, T. M. Kardaś, and Y. Stepanenko, "Real-time observation of double-Hopf bifurcation in an ultrafast all-PM fiber laser," *Laser Photonics Rev.* **16**(10), 2100646 (2022).
48. J. Zou et al., "Towards visible-wavelength passively mode-locked lasers in all-fibre format," *Light-Sci. Appl.* **9**, 61 (2020).
49. M. A. Hall, J. B. Altepeter, and P. Kumar, "Ultrafast switching of photonic entanglement," *Phys. Rev. Lett.* **106**(5), 053901 (2011).
50. H. Wu et al., "Ultra-high speed random bit generation based on Rayleigh feedback assisted ytterbium-doped random fiber laser," *Sci. China-Technol. Sci.* **64**(6), 1295–1301 (2021).
51. Z. Hu et al., "Simulation of the generation conditions and influence parameters of a self-mode-locked erbium-doped fiber laser," *Opt. Express* **31**(4), 5882–5892 (2023).
52. K. Li et al., "Real-time observation of stationary and pulsating noise-like vector pulses in a fiber laser," *Opt. Express* **31**(14), 23406–23418 (2023).

Ming Shen received his BS degree from the University of Electronic Science and Technology of China, Chengdu, China, in 2019. He is currently pursuing his PhD in Wuhan National Laboratory for Optoelectronics, Huazhong University of Science and Technology, Wuhan, China. His research interests include random fiber lasers and femtosecond laser writing.

Yanxin Li received her BS degree from the Changchun University of Science and Technology, Changchun, China, in 2019. She is currently working toward a PhD in the Wuhan National Laboratory for Optoelectronics, Huazhong University of Science and Technology, Wuhan, China. Her research focuses on optics turbulence and fiber lasers.

Qianying Li received her BS degree from the Hubei University of Technology, Wuhan, China, in 2017 and her MS degree from the University of Sydney, Sydney, Australia, in 2020. She is currently working toward a PhD in Wuhan National Laboratory for Optoelectronics, Huazhong University of Science and Technology, Wuhan, China. Her research interests focus on fiber lasers.

Xuewen Shu (a senior member, IEEE; fellow, Optica) received his PhD from the Huazhong University of Science and Technology, Wuhan, China, in 2000. He is currently a full professor at the Wuhan National Laboratory for Optoelectronics, Huazhong University of Science and Technology, Wuhan, China. His research interests include fiber gratings, optical fiber communications, fiber lasers, and optical fiber sensors.